Performance of the ATLAS liquid argon forward calorimeter in beam tests

2013 JINST 8 P05006

(http://iopscience.iop.org/1748-0221/8/05/P05006)

PUBLISHED BY IOP PUBLISHING FOR SISSA MEDIALAB

RECEIVED: *February 21, 2013*
ACCEPTED: *April 10, 2013*
PUBLISHED: *May 16, 2013*

Performance of the ATLAS liquid argon forward calorimeter in beam tests

J.P. Archambault,[a,1] **A. Artamonov,**[b] **M. Cadabeschi,**[c] **V. Epshteyn,**[b] **C. Galt,**[c,2] **D. Gillberg,**[a,3] **P. Gorbounov,**[c,4] **L. Heelan,**[a,5] **M. Khakzad,**[a,6] **V. Khovanskiy,**[b] **P. Krieger,**[c,7] **P. Loch,**[d] **T.G. McCarthy,**[a] **F.G. Oakham,**[a,8] **R.S. Orr,**[c] **J. Rutherfoord,**[d] **A. Savine,**[d] **M. Schram,**[a] **P. Shatalov,**[b] **L. Shaver,**[d,9] **M. Shupe,**[d] **V. Strickland,**[a,4] **P. Thompson**[c] **and I. Tsukerman**[b]

[a]*Physics Department, Carleton University, Ottawa, Ontario, K1S 5B6, Canada*
[b]*ITEP Moscow, 117 218 Moscow, Russia*
[c]*Physics Department, University of Toronto, Toronto, Ontario, M5S 1A7, Canada*
[d]*Physics Department, University of Arizona, Tucson, Arizona, 85721, U.S.A.*

E-mail: krieger@physics.utoronto.ca

2013 JINST 8 P05006

[1]Now at the Canadian National Research Council, Ottawa, Canada.
[2]Now at the U.S. Patent and Trademark Office, Alexandria, Virginia, 22313, U.S.A.
[3]Now at CERN, Geneva, Switzerland.
[4]Permanent Address, ITEP, Moscow.
[5]Now at University of Texas at Arlington, Arlington, Texas, 76019, U.S.A.
[6]Now at School of Particles and Accelerator Inst. for Res. in Fundamental Science, Tehran, Iran.
[7]Corresponding author.
[8]Also at TRIUMF, Vancouver, BC, V6T 2A3, Canada.
[9]Retired.

doi:10.1088/1748-0221/8/05/P05006

ABSTRACT: One of two ATLAS Forward Calorimeters, consisting of three modules, one behind the other, was exposed to particle beams of known energies in order to study the detector performance with and without the presence of upstream material in the beam, and at the inner edge of the acceptance where shower energy containment is incomplete. Data were taken in the H6 beamline at CERN using electron and hadron beams with energies from 10 to 200 GeV. Results related to the intrinsic detector calibration, based on data taken with a minimal amount of material in front of the detector, have been previously published, but are updated here. This paper focuses on studies of data taken with additional upstream material in place. The effects of this additional material on the linearity and resolution of the response are presented. The response at the inner edge of the acceptance is also investigated. For all analyses, results based on a GEANT4 simulation of the beam-test setup and detector response are also presented.

KEYWORDS: Noble liquid detectors (scintillation, ionization, double-phase); Calorimeters; Large detector systems for particle and astroparticle physics; Detector modelling and simulations I (interaction of radiation with matter, interaction of photons with matter, interaction of hadrons with matter, etc)

2013 JINST 8 P05006

Contents

1 Introduction

ATLAS [1] is one of the two general purpose detectors designed to record the products of high-energy proton-proton collisions at the Large Hadron Collider (LHC) at CERN [2], at luminosities up to $10^{34}\,\mathrm{cm}^{-2}\mathrm{s}^{-1}$. The energy and flux density of particles produced in these collisions are largest near the directions of the incident beams. This harsh environment close to the accelerator beam pipe places severe constraints on the detector elements designed to operate there. The ATLAS Forward Calorimeters (FCals) sit about 4.7 m from the interaction point, close to the beamline, extending the calorimetric coverage from a pseudorapidity, $|\eta|$, of about 3.1 to 4.9. Since tracking in ATLAS extends only to $|\eta| = 2.5$, in-situ calibration techniques relying on tracking cannot be employed. For that reason, calibration of the FCal using beam-test data is especially important. The intrinsic performance of the detector was reported on in a previous publication [3], which also provided a detailed description of the beam-test setup. That paper focused on the linearity and resolution of the response to electrons and pions in the case where the amount of material in front of the calorimeter was minimized. The effect of material present between the interaction point and the FCal in the ATLAS environment was not accounted for, nor were the results compared to Monte Carlo (MC) simulations. Both of these issues are relevant for a complete understanding of the performance of the FCal that is now installed and operating in ATLAS. These topics are the focus of this paper.

2013 JINST 8 P05006

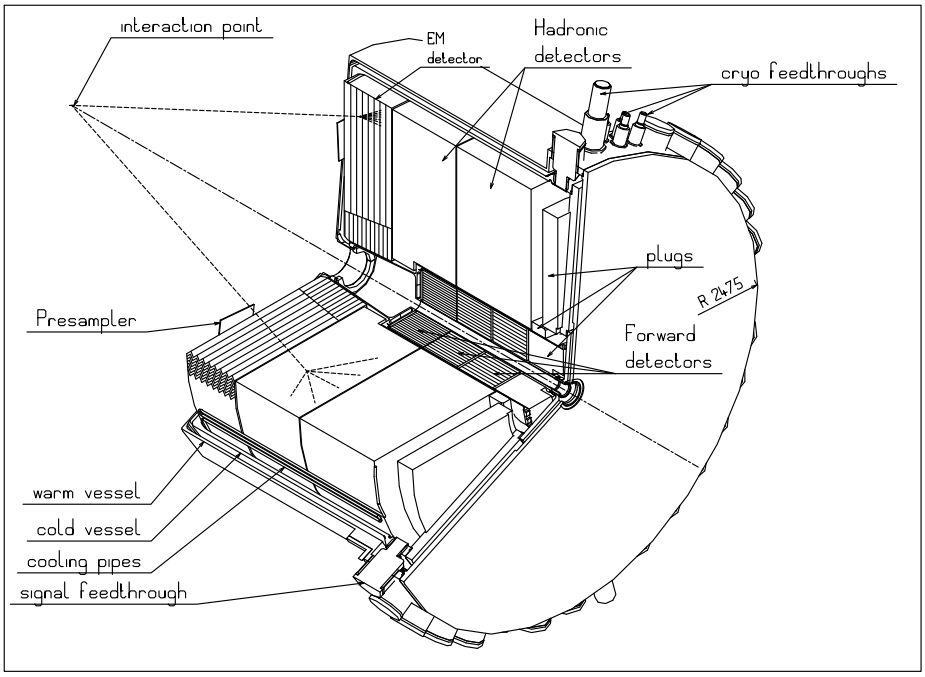

Figure 1. A schematic cutaway view of the ATLAS endcap cryostat, showing the location of the forward calorimeter relative to the other endcap calorimeters [4].

Each FCal consists of three modules, referred to as FCal1, FCal2 and FCal3, with a total depth of about 10λ. The FCal1, a copper module, is closest to the interaction point. Behind it are the FCal2 and FCal3, respectively, which are made mainly of tungsten in order to optimize both longitudinal and transverse hadronic shower containment in the available space. The location of the FCal within the LAr endcap calorimeter system is illustrated in figure 1. A cross-sectional view of the upper half of the FCal in this environment is shown in figure 2, which more clearly illustrates its position relative to the other endcap calorimeters, and shows some of the material located between the FCal and the ATLAS interaction point (IP). Behind the FCal3, an un-instrumented copper-alloy plug provides additional shielding for the muon system. In ATLAS, the FCal sits within a cylindrical support tube with a cone-shaped extension (the "forward cone") on the IP side that bolts to the front face of the endcap cryostat. A cryostat bulkhead made of 5 cm thick aluminum is located just in front of the FCal1. The ATLAS JM moderator shield (labeled "Poly Shield" in figure 2) is designed to reduce albedo from the calorimeter back into the inner detector [1]. This shielding consists of a tube of outer radius 178.5 mm and 38.5 mm thickness, extending for just over a meter in front of the FCal, and an 80 mm thick plug with inner and outer radii of 74.5 mm and 178.5 mm, concentric with the beamline and situated just upstream of the cryostat bulkhead.

In order for the FCal to operate in the very high-flux environment at the LHC, the liquid argon (LAr) gaps must be much smaller than the 1–2 mm that is traditional in a LAr calorimeter. This constraint is accommodated by using thin annular LAr gaps oriented parallel to the beamline. Electrodes are formed by inserting an absorber rod, which serves as the anode, into a copper tube which acts as the cathode. The rod is positioned concentrically using a helically-wound radiation

2013 JINST 8 P05006

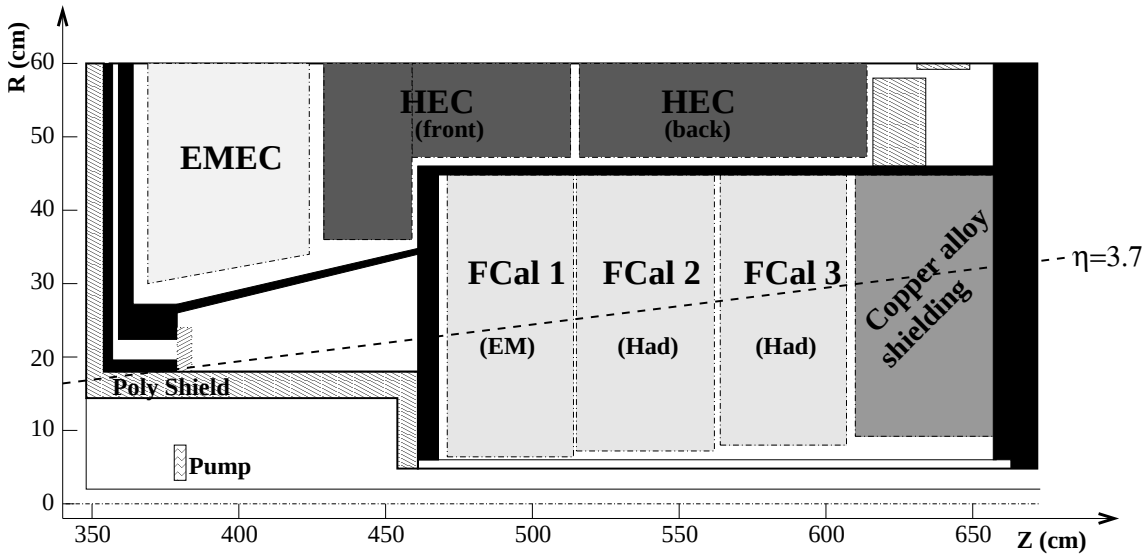

Figure 2. A cross-sectional view of the upper half of the forward calorimeter, in the cryostat support tube which houses it. Cryostat walls are shown in black. Particles at $|\eta| \approx 3.7$ (shown) must traverse both the the tube portion of the polyethylene shielding and the cryostat bulkhead. At higher $|\eta|$ there is additional material, for instance the plug portion of the Poly Shield as well as a metal pump, also illustrated.

hard plastic (PEEK) fibre that maintains the narrow (269 μm in the FCal1) LAr gap and electrically separates the anode and cathode. These electrodes are arranged in a hexagonal pattern within an absorber matrix, leading to a detector with a fine lateral segmentation that can be exploited in the event reconstruction. For high voltage distribution and signal readout, electrodes are ganged together, in groups of 4/6/9 for the FCal1/2/3, using interconnect boards at the readout face of each module. In each module, readout channels correspond to four such electrode groups over most of the detector volume; at the inner and outer peripheries, readout channels are formed by single electrode groups.

This paper describes the performance of one of the two final ATLAS forward calorimeters for single particles, i.e. electrons and pions, over the energy range of about 10–200 GeV, in an environment in which some of the material located upstream of the FCal in the ATLAS environment has been modelled. Details of the design and construction of the detector can be found in reference [5]. Details on the ATLAS detector, including information on the material that sits between the ATLAS interaction point and the front face of the FCal, can be found in [1]. Only material associated with the endcap calorimeter (as illustrated in figure 2) has been modelled in the simulation results presented here.

Section 2 briefly describes the goals of the beam test, the experimental setup, and the Monte Carlo simulation infrastructure. Analysis of the data and Monte Carlo samples for both electrons and pions is described in section 3. Section 4 briefly compares the results to similar results obtained from a separate beam test designed for study of the combined performance of the endcap and forward calorimeters. A summary and conclusions are provided in section 5.

2013 JINST 8 P05006

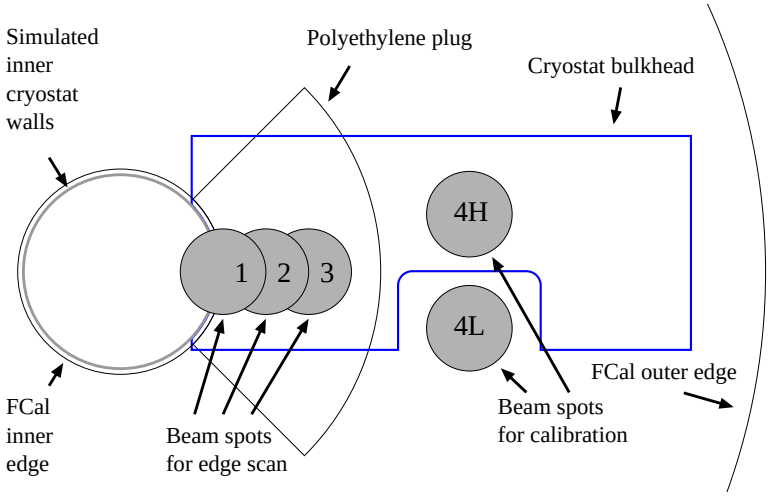

Point	angle	$\lvert\eta\rvert$
1	0.88°	4.9
2	1.25°	4.5
3	1.61°	4.3
4	2.98°	3.7

Figure 3. A view of the region of the FCal instrumented for the beam test. The five beam impact point regions are illustrated, as are an aluminum plate used to simulated the cryostat bulkhead and a polyethylene piece simulating the plug portion of the ATLAS JM moderator near the beam hole. The beam impact angle at each point is listed in the table.

2 Experimental setup

2.1 Beam test overview

The FCal beam-test setup and recorded datasets are described in detail in reference [3] and briefly below. The aims of this beam test were:

- to determine the FCal energy calibration;
- to study the FCal performance in the presence of upstream material;
- to study the performance for particles near the inner radius (high-$|\eta|$ region) of the FCal, where energy leakage down, and/or "splashing" across the beam-hole becomes relevant.

Note that studies of the performance at the outer (low-$|\eta|$) edge were done in a separate beam test [6, 7] using a setup involving the other LAr endcap calorimeter subsystems, since an understanding of the calorimeter performance in this region involves an understanding of the energy sharing between the different calorimeter subsystems (see figure 2) and of the energy lost in the crack region between them.

Different beam-test conditions were used for investigation of the topics of interest here; in particular, different beam impact points were used. These are shown in figure 3 which also illustrates the locations of some of the simulated upstream material. There are two points (4L, 4H) at positions corresponding to $|\eta| \approx 3.7$ where shower energy containment is maximal, and three overlapping beam spots (1, 2, 3) close to the inner edge that were intended for a study of the response in this difficult region where energy can escape down or splash across the beam-hole. Previously published results on the energy calibration relied on analysis of the data taken at the 4L position, where the amount of upstream material was minimized. For all other impact points, upstream material associated with the endcap cryostat was modelled, as described later in this section. This paper

2013 JINST 8 P05006

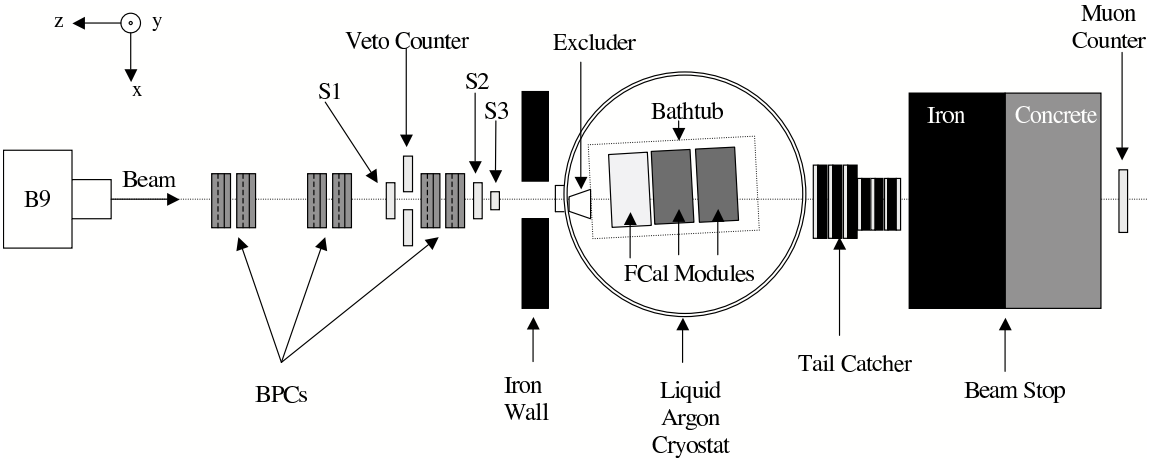

Figure 4. Schematic of the beamline setup for the FCal calibration beam test (not to scale).

focuses on the results obtained from an analysis of data taken at the 4H impact point, in order to investigate the effects of the upstream material on the detector performance. Results are compared to simulations in order to evaluate the ability of the simulation to model the detector performance as well as the effects, on the performance, of the upstream material. In section 3.6 results from analysis of the inner-edge-scan data are also presented.

As mentioned above, for the datasets under discussion here, an attempt was made to simulate some of the conditions at ATLAS, where particles at $|\eta| \approx 3.7$ traverse a substantial amount of material before reaching the FCal, such as the cryostat bulkhead and the tube portion of the ATLAS JM shielding; the latter represents a large thickness of borated polyethylene at these incident angles. In ATLAS there is also material associated with the inner detector and associated services. However, at the time of the beam test, the amount of this material was not well known, and since it was expected to vary strongly with η and ϕ, no attempt was made to simulate it.

The original plan for the beam test was to use a completed FCal installed in its support tube. However, delays in the availability of the tube made this impractical. Instead a purpose-built stand was constructed to hold the production modules of the FCal for the C-side of ATLAS. These were positioned with close-to-nominal spacing, and the separations and any small relative rotations were surveyed after installation. To protect the modules against any debris left after cleaning of the cryostat (which might induce HV shorts in the very narrow liquid argon gaps) the detector stand, with the three modules installed, was placed into a "bathtub" made of 1.5 mm thick stainless steel. This had several holes covered with a fine stainless steel mesh to allow LAr to flow in during filling of the cryostat. The LAr fill was controlled to maintain a level below the top of the bathtub.

Modelling the material of the local upstream environment meant modelling the cryostat bulkhead and the tube and plug portions of the ATLAS JM moderator. The tube region was modelled by placing polyethylene in the beamline upstream of the cryostat, in the slot of an iron wall located just upstream of the cryostat (see figure 4), while the plug portion, relevant only for positions 1–3, was modelled with a polyethylene piece mounted to the outside of the front-face of the bathtub. The cryostat bulkhead was modelled using 5.0 cm of aluminum, bolted to the inside wall of the bathtub, with a cut-away around the 4L position. The material mounted on the bathtub wall is il-

2013 JINST 8 P05006

lustrated in figure 3. At position 1, the innermost scan point, an ion pump that sits in the evacuated region of the forward cone, was modelled with a small 30 mm-thick aluminum block placed in the beamline about 900 mm upstream of the detector. In ATLAS, the inner bore of the FCal (referred to here as the beam-hole) is occupied by the LHC beam-pipe. For the beam test, a thin-walled sealed stainless steel cylinder was used to exclude LAr from this region. This is important only for the inner-edge studies. An excluder made of Rohacell was placed between the inner wall of the cryostat and the outer wall of the bathtub. However, there was no excluder between the inner wall of the bathtub and the FCal1 front face, 15 cm downstream of it. In the 4H position, 5 cm of this depth was occupied by the aluminum plate used to model the cryostat bulkhead. In ATLAS the nominal thickness of this volume of LAr is 29 mm.

2.2 Beamline instrumentation

The beam-test setup and beamline instrumentation are illustrated in figure 4 and described in detail in reference [3]. Briefly, it contained several scintillators used for triggering, including one with a 6.5 cm diameter circular cut-out used as a veto-counter. The wide beam profile was chosen in order to average over beam-particle impact points on the calorimeter, since the response is known to have some dependence on the impact point relative to the nearest electrode: e.g. the response to particles arriving at the calorimeter front face near the center of an electrode rod is lower than that of particles that hit the calorimeter front face near the LAr gap [8]. The impact point of each beam particle is reconstructed using information from a set of Beam Position Chambers (BPCs) to extrapolate the beam tracks to the front face of the FCal. A CEDAR [9] counter, located in the H6 beamline upstream of the instrumentation illustrated in figure 4, provided particle identification information which was mainly used for proton-pion separation in the hadron data. Downstream of the cryostat was a steel/scintillator tail-catcher, to provide measurements of any leakage out of the back of the FCal, and an iron/concrete beam stop, behind which was a muon counter. The aperture of this counter was insufficient to provide coverage for all scattered muons, especially at the lowest energies, so information from the tail-catcher was also required for the efficient suppression of muons. Beam particles were selected using a set of "beam cleaning" requirements as described in reference [3], based on information from all of the beamline detectors.

2.3 GEANT4 Monte Carlo simulation

The beam-test setup has been modelled using GEANT4 [10] (version 4.9.2), with the FCal detector description extracted from the ATLAS detector simulation package, with a small (5%) adjustment to the density of the electrode rod material in the hadronic modules, to better reflect the measured value. The simulation of the ATLAS Liquid Argon Calorimeter is described in detail in reference [11]. As is the case in ATLAS, all simulations of the forward calorimeter, with its narrow LAr gaps, use a GEANT4 range cut of 30 μm. For the beamline detectors (scintillators, tracking chambers) only the material is modelled; no signals are formed. Particles are generated starting at the position of the vertical deflection magnet (B9) about 32 m upstream of the FCal and transported through the materials of the beamline and the cryostat and bathtub walls, to the detector. For the results presented here this was done using a beamspot of roughly 6.5 cm diameter, to match the acceptance of the hole-veto counter. For most simulations, the beamspot was uniformly populated: while the beam profile in the data was not uniform, it varied slowly over the acceptance

2013 JINST 8 P05006

and studies show that modelling the true beam profile does not significantly affect the results for positions 4L and 4H which are far from the inner edge. This is not the case for simulations related to the inner-edge studies, as will be discussed in section 3.6.

For the FCal, the energy deposited in the LAr gaps is converted into ADC counts using the previously published EM-scale factors for each module. Using the known pulse shape, this information is used to generate the digitized pulse-shape samples expected by the ATLAS reconstruction chain. Since the noise in the data was not constant over the full period of the beam test [3], for each Monte Carlo sample (beam type, beam energy) electronics noise is then added channel-by-channel, based on the values obtained from the set of data runs used for that beam type and energy, with correlations taken into account. The resulting Monte Carlo samples were then reconstructed and analyzed in the same way as the data.

For modelling of the data taken at positions 1, 2, 3 and 4H, the upstream material described in section 1 was included in the simulation. The beam-hole region of the FCal was modelled as a stainless steel cylinder with dimensions matching those of the cylinder used to keep this region free of liquid argon; the interior of the cylinder was modelled as vacuum.

For simulation of pions, three different GEANT4 physics lists were investigated: QGSP_BERT, QGSP_BERT_HP and FTFP_BERT. The first of these is the default for ATLAS simulations. The second is the same model but with high-precision modelling for low-energy neutrons. The third uses a different model for the high-energy inelastic pp collisions. Use of the QGSP_BERT_HP physics list was in part motivated by studies showing large differences, relative to QGSP_BERT, in the modelling of hadronic showers in tungsten [13].

3 Data analysis

3.1 Overview

This paper focuses on a comparison of results obtained from analyses of the data taken at the 4L and 4H positions, in order to investigate the effects, on the performance, of the material upstream of the FCal. Results from both datasets are also compared to Monte Carlo simulations in order to investigate the simulation's ability to model both the intrinsic performance of the detector and the effects of the upstream material. Cell-level signal reconstruction was done using the OFC technique [12] that is used in ATLAS and described in our previous publication [3]. Since that publication, a small problem with the beam-test implementation of the energy reconstruction was discovered and fixed. In order to properly evaluate the effects of the upstream material by comparison of the results at the 4L and 4H positions, the 4L results are updated here; the analysis of both datasets is the same as the published one[1] except for the one bug fix and the removal of CEDAR requirements (used for pion-proton separation) in the analysis of data taken using negatively-charged hadron beams. As in the previous study, for both electrons and pions a cylindrical clustering technique was used, in which the reconstructed energy in each module was obtained by summing the energies of all channels within a certain radial distance of the beam-particle impact point, obtained by extrapolation of beam particle tracks reconstructed from the BPC data. Distances were calculated based on the center of each readout channel. For electromagnetic showers, about 99% of the energy is

[1] A more recent release of the ATLAS Athena software framework was used.

2013 JINST 8 P05006

deposited within an 8 cm cylinder centred on the electron impact point on the face of the FCal1 module. For pions, a larger cylinder is required for containment of the broader hadronic showers, and cells from all three modules must be clustered. Contributions from any residual hadron contamination in the electron data are modelled using hadron data taken at the same energy, though studies show that the results do not depend much on such a detailed treatment of this background. When analyzed for this purpose, the hadron data were reconstructed with the same cylinder radius as used for electrons.

Analysis of the inner-edge-scan data (positions 1, 2 and 3) was done using the same cell-level reconstruction, but a different clustering algorithm, since the cylindrical clustering procedure is ill-defined in the region near the inner edge. The topological-clustering algorithm [14] used for this analysis is the default clustering algorithm used for hadronic energy reconstruction in ATLAS and is also investigated for the 4L and 4H datasets in section 3.5.

Below, the electron analyses are first discussed, along with the predictions of the corresponding Monte Carlo simulations. Following that, the analysis of the data taken with hadron beams is presented. In each case, results are presented for both the 4L and 4H datasets. An investigation of simple electromagnetic and hadronic shower shape distributions is discussed in section 3.4, mainly for validation of the Monte Carlo simulations. Section 3.5 introduces the topological clustering algorithm and investigates its performance for electron and pion energy reconstruction at the 4L and 4H points. Finally, in section 3.6 the results of the analysis of the data from the inner-edge scan are presented.

3.2 Analysis of electron data

Beam particles were selected as described in [3]. For accepted events, the energy reconstruction in each of the FCal modules was performed as described above. The results for the response to electrons were obtained using 8 cm cylindrical clustering of FCal1 cells. The expected signal shape is slightly non-Gaussian due to the impact point variation of the FCal response, discussed earlier; this effect is most pronounced at higher energies. As in the previously published analysis, the reconstructed energy spectrum is fitted with a function consisting of the sum of a double Gaussian, parametrizing the signal, and a description of the hadron contribution, with a shape obtained from analysis of the hadron data (taken at the same energy and position) and a normalization that is allowed to float. Fits that do not model this background yield very similar results. As a systematic study, the double-Gaussian fit was performed in two ways. In the first, all six parameters were allowed to vary in the fit. In the second, at all energies, the ratio of the means of the two Gaussians and the relative populations were constrained to have the values obtained from the fit to the 200 GeV data. The latter constraint is motivated by the hypothesis that the relative population of the two Gaussians is dominantly determined by the geometry of the unit cell, i.e. the relative populations of different beam-particle impact points with respect to the centre of the closest electrode. These two fit procedures yield almost identical results. A single-Gaussian parametrization was also examined. This provides a much poorer fit in the signal region, but the extracted signal parameters are not dramatically affected. Each fit was done over the full range of reconstructed energies, excluding the region near zero where muons can contribute. The reconstructed energy and resolution are determined from the parameters of the two Gaussians fitted to the signal peak. The background treatment used requires the existence of a hadron dataset taken at the same energy and position.

2013 JINST 8 P05006

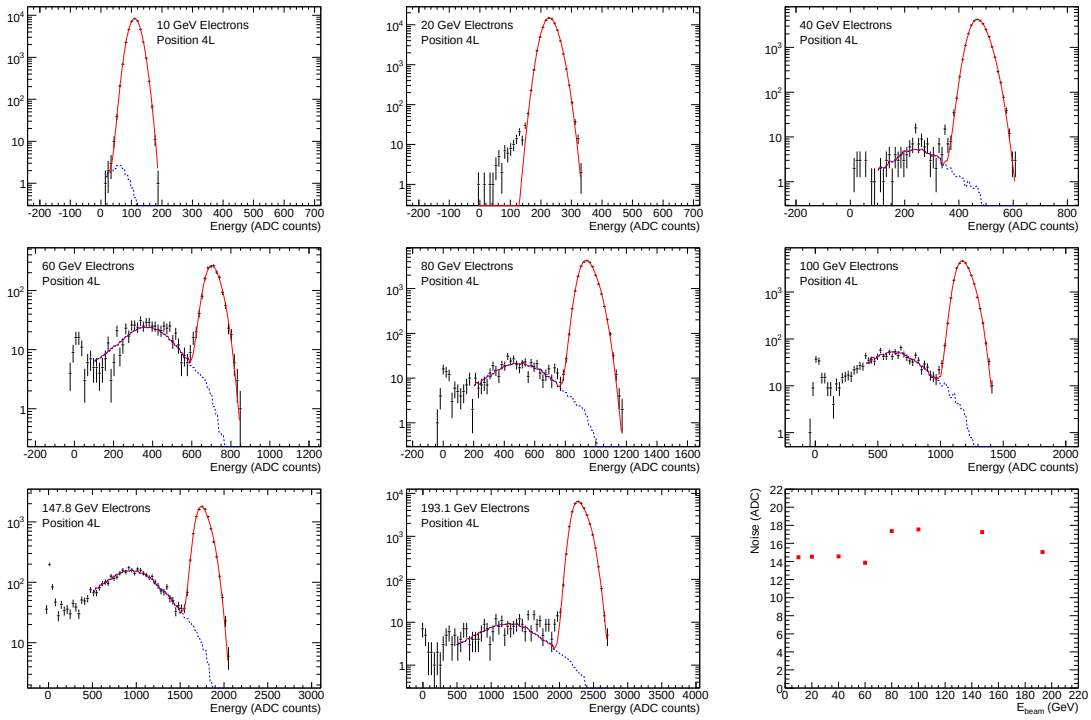

Figure 5. Energy spectra from electron data at 4L, obtained using an 8 cm cylinder sum. In each case the points represent the data, the solid line shows the results of the fit described in the text while the dotted line shows just the fitted contribution of the hadronic background. The plot at the bottom right shows the reconstructed noise for each 4L energy point.

However, 20 GeV hadron samples are not available at either the 4L or 4H position. The results of the analysis at each of the beam energies are shown in figures 5 and 6 for the 4L and 4H data, respectively. The results of the fits are overlaid. In the case of the 20 GeV data the fit function was a double Gaussian only, since no hadron data was available. However, the tail to lower energy is small in this case. Results are presented using a logarithmic vertical scale in order to clearly display the tails of the distribution. Also shown in the lower-right plot of each figure is the noise contribution for each energy point, obtained by clustering cells from randomly-triggered events from the same data runs. This varies from point to point due to the time-dependence mentioned earlier.

In the case of the analysis of the 4L data, these results update those that were previously published [3], which were used for determination of the FCal1 electromagnetic scale factor. The response linearity and (noise-subtracted) resolution extracted from these distributions are shown in figures 7 and 8 respectively. At the 4L position, the electromagnetic scale factor (ADC $\rightarrow$ GeV) is (12.0 ± 0.1) compared to the previously published value of $(12.07 \pm 0.07 \pm 0.07)$. The $\sim 1\%$ difference is due to the energy-reconstruction bug mentioned earlier, which resulted in a small systematic underestimation of the energy, due to a rounding error on the result of the signal amplitude reconstruction with the OFCs. As was the case for the published results, the fit yields a slightly negative intercept (-9.6 ± 0.1 ADC counts), which is attributed to energy losses in the beamline, including those that occur upstream of the B9 magnet (which are not modelled in the simulation).

2013 JINST 8 P05006

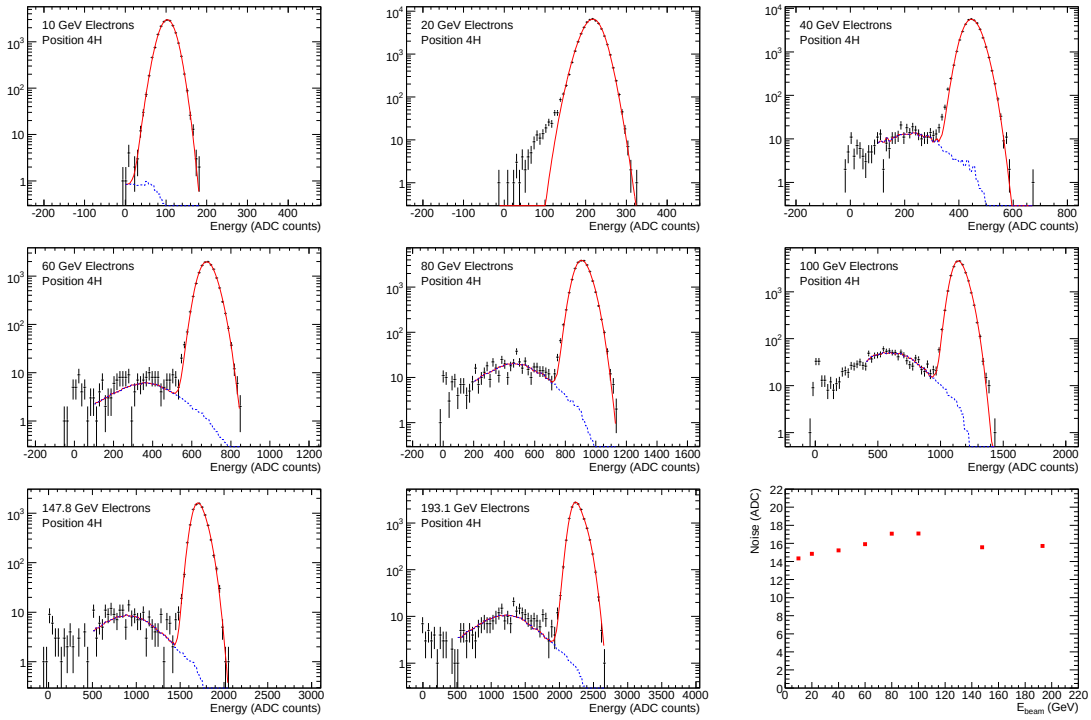

Figure 6. Energy spectra from electron data at 4H, obtained using an 8 cm cylinder sum. In each case the points represent the data, the solid line shows the results of the fit described in the text while the dotted line shows just the fitted contribution of the hadronic background. The plot at the bottom right shows the reconstructed noise for each 4H energy point.

The residuals from the linear fit are also shown; the plotted errors are dominated by systematic uncertainties, evaluated as described in reference [3], which are mainly due to imperfect knowledge of the beam energies, and the choice of clustering radius. For the linearity at position 4H, a slightly smaller EM scale factor is obtained, along with a slightly more negative intercept (-17.5 ± 0.1 ADC counts). The change in the intercept of the linear fit, due to energy lost in the upstream material, is similar in data and Monte Carlo, and corresponds to an additional upstream energy loss of about 700 MeV for electrons at 4H. The fit residuals at the 4L and 4H positions, shown in figure 7, are within 1% except for the lowest energy point at the 4H position. The simulation results indicate a small bias for the lowest energy point, which may account for some of the deviation from linearity seen for the data in this region.

For the resolution, the noise-subtracted distributions are fitted to a parametrization of the form

$$\frac{\sigma_E}{E} = \frac{b}{\sqrt{E}} \oplus c\,.$$

At position 4L, the fit yields $b = (27.0 \pm 0.9)\%\sqrt{\text{GeV}}$ and $c = (3.6 \pm 0.1)\%$ respectively, where the quoted errors include statistical (see table 1) and systematic uncertainties. These are to be compared to the previously published values of $(28.5 \pm 1.0)\%\sqrt{\text{GeV}}$ and $(3.5 \pm 0.1)\%$. The quoted uncertainties are, in each case, dominated by systematics associated with variation of the beam particle selection criteria and the fit parametrization used for extraction of the signal parameters.

2013 JINST 8 P05006

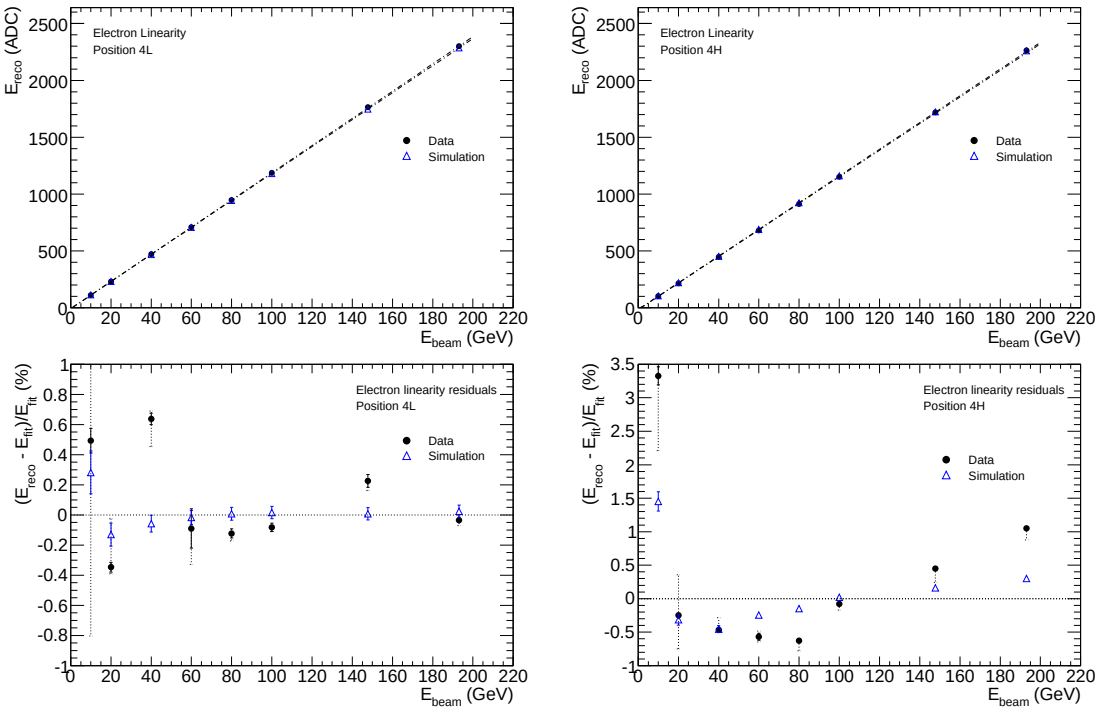

Figure 7. The upper plots show the response linearity for electrons, from analysis of data taken at positions 4L and 4H, with the results of a linear fit overlaid. The lower plots show the corresponding residuals. Monte Carlo predictions are also shown.

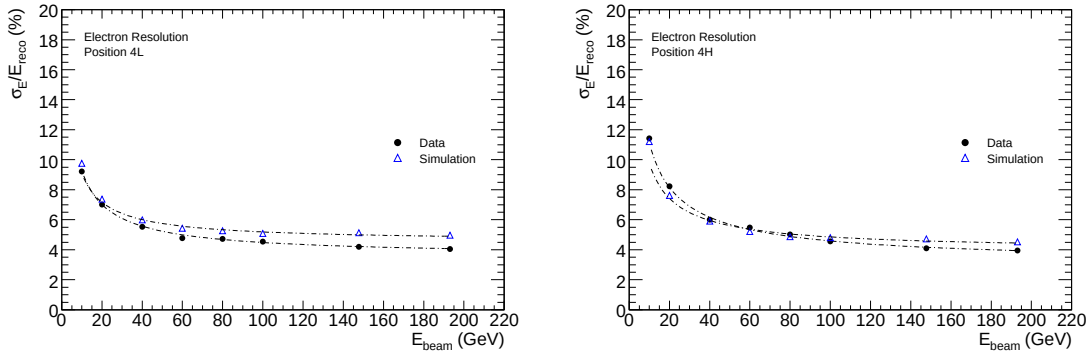

Figure 8. Resolution of the FCal response to electrons, as a function of beam energy, from analysis of data taken at positions 4L and 4H. Simulation results are also shown, and fit results are overlaid. The errors shown are statistical only.

At position 4H one expects some degradation in the stochastic term due to fluctuations in the energy loss in the upstream material. This is observed, with the stochastic term increasing from $(27.0 \pm 0.9)\%\sqrt{\text{GeV}}$ to $(33.7 \pm 0.8)\%\sqrt{\text{GeV}}$. The constant term is slightly smaller than at 4L, possibly due to early showering in the upstream material which may slightly reduce the effect of the impact point dependence of the response. The plots also show the results of the simulations, which predict poorer resolution at high energies than is actually achieved. The resolution distributions have all been fitted to the parametrization described earlier; the results are summarized in

2013 JINST 8 P05006

Table 1. Results of fits to electron energy resolution results for data and Monte Carlo at 4L and 4H. Quoted errors are statistical only. Systematic uncertainties are described in the text.

	Stochastic term ($\%\sqrt{\text{GeV}}$)		Constant term (%)	
	4L	4H	4L	4H
Data	27.0 ± 0.2	33.7 ± 0.2	3.58 ± 0.02	3.11 ± 0.03
Simulation	24.7 ± 0.3	28.1 ± 0.3	4.56 ± 0.03	3.96 ± 0.03

table 1. At both positions, the stochastic term from the simulation is lower than observed in data; the constant term, however, is slightly higher. The relative increase in the stochastic term when comparing the 4H results to those at 4L is larger in data than in Monte Carlo, while the relative decrease in the constant term is in good agreement. The difference in the constant terms derived from data and Monte Carlo is similar to that seen in a previous beam test [8], which presented resolution results for electrons over the same range of energies investigated here. That test used a prototype FCal1 module and compared results to predictions from both GEANT3 and GEANT4. The electron resolution at high energy was shown to be well described by the GEANT3 simulation, while the GEANT4 simulation predicted a poorer resolution than seen in the data, by an amount similar to that presented here. For the present analysis, checks were done to see whether the larger constant term in Monte Carlo might be related to a mis-modelling, in simulation, of the impact-point dependence of the detector response. At the highest energy point, where the discrepancy is largest, this was found not to be the case. Reweighting the Monte Carlo sample (193 GeV electrons at position 4L) to account for the slightly different impact-point dependence observed in data reduces the prediction for the relative energy resolution only slightly, from $4.97 \pm 0.03\%$ to $4.86 \pm 0.01\%$.

3.3 Analysis of hadron data

For the hadron data, the energy reconstruction involves the combination of the energy deposited in the three individual FCal modules, each of which has a different sampling fraction and thus a different electromagnetic scale. Each module additionally has a different relative response to electrons and hadrons. Both effects must be accounted for when combining information from the three modules for the reconstruction of the total hadronic energy. In the present and previously published analysis, this is done using a simple "flat-weighting" technique in which the energy is reconstructed from cells within a 16 cm radius of the beam-particle impact point, as a sum of the form

$$E = g_1\alpha_1(\text{ADC}_{\text{FCal1}}) + g_2\alpha_2(\text{ADC}_{\text{FCal2}}) + g_3\alpha_3(\text{ADC}_{\text{FCal3}}) \tag{3.1}$$

where α_1, α_2 and α_3 are the (ADC $\rightarrow$ GeV) electromagnetic scale factors for the three modules and g_1, g_2 and g_3 are chosen to minimize the energy resolution, with the constraint that the average reconstructed energy equal the known beam energy. Because particles hit the calorimeter at an angle, the impact points around which the clustering is performed are obtained by projecting the particle track to the front face of each of the three modules.

The flat weights are derived separately at each energy and are shown for each module, as a function of energy, in figure 9, for both the 4L and 4H analyses, along with the predictions from

2013 JINST 8 P05006

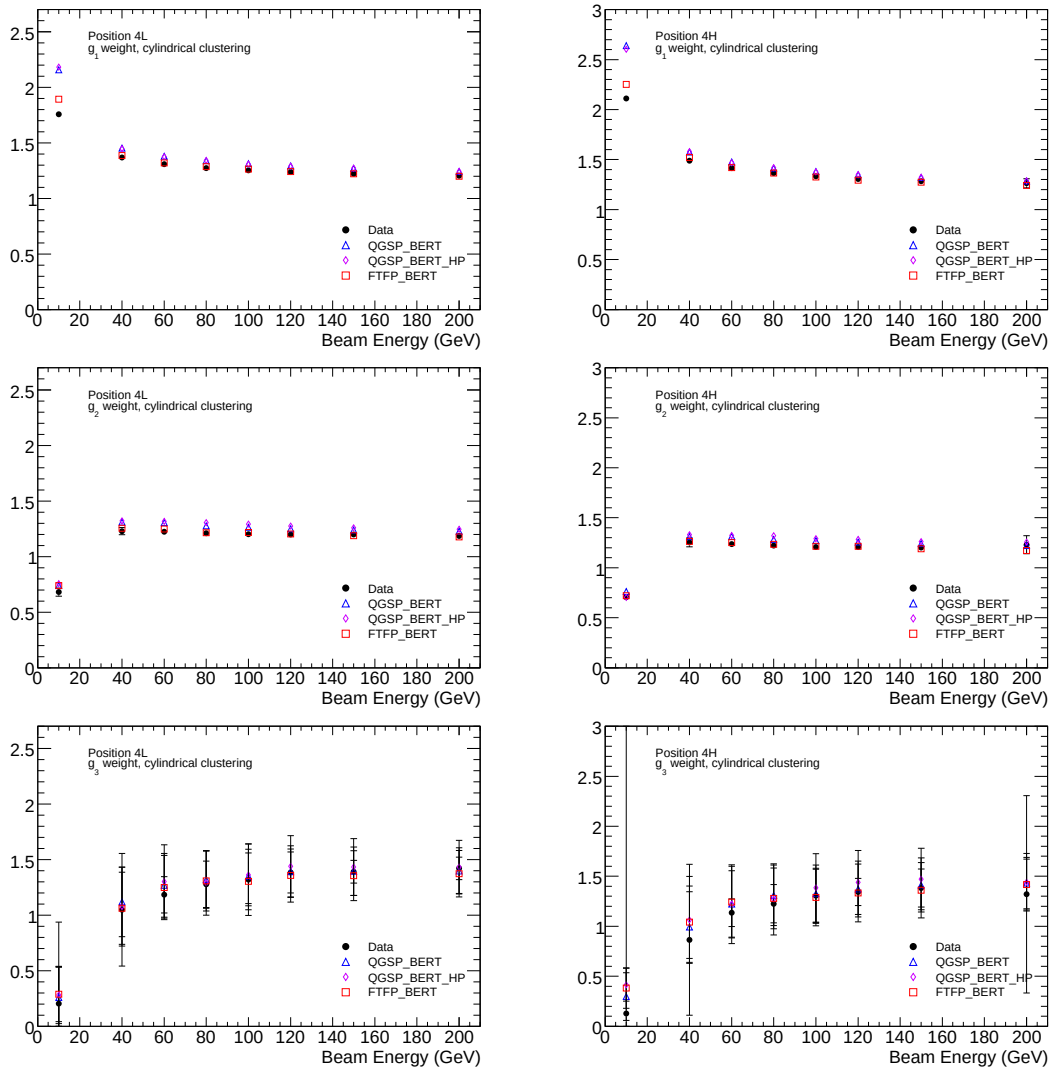

Figure 9. Flat weights for hadronic energy reconstruction, derived from the data, at each energy point. The predictions of the simulation are also shown. These results are for the cylindrical clustering procedure described in the text.

simulations, using each of the three hadronic physics lists. In general the data/MC agreement is quite good. This is not the case for the lowest energy point in the FCal1, and the low energy deposits in the FCal3 lead to rather large uncertainties on the g_3 values. The energy-dependence is seen to be rather weak at higher energies.

Since energy-dependent weights can anyway not be used at ATLAS, a single set of weights is used for the reconstruction at all energies. In ATLAS, most of the jets in the FCal have very high energy, so the results presented below were obtained using the weights derived from the highest-energy (200 GeV) data sample. The spread of results obtained using the weights derived from the four highest energy points is considered in the evaluation of the systematic uncertainties.

Figures 10 and 11 show the distributions of reconstructed energy at each beam energy, for pions selected from the hadronic data taken at the 4L and 4H positions, in each case using the flat

2013 JINST 8 P05006

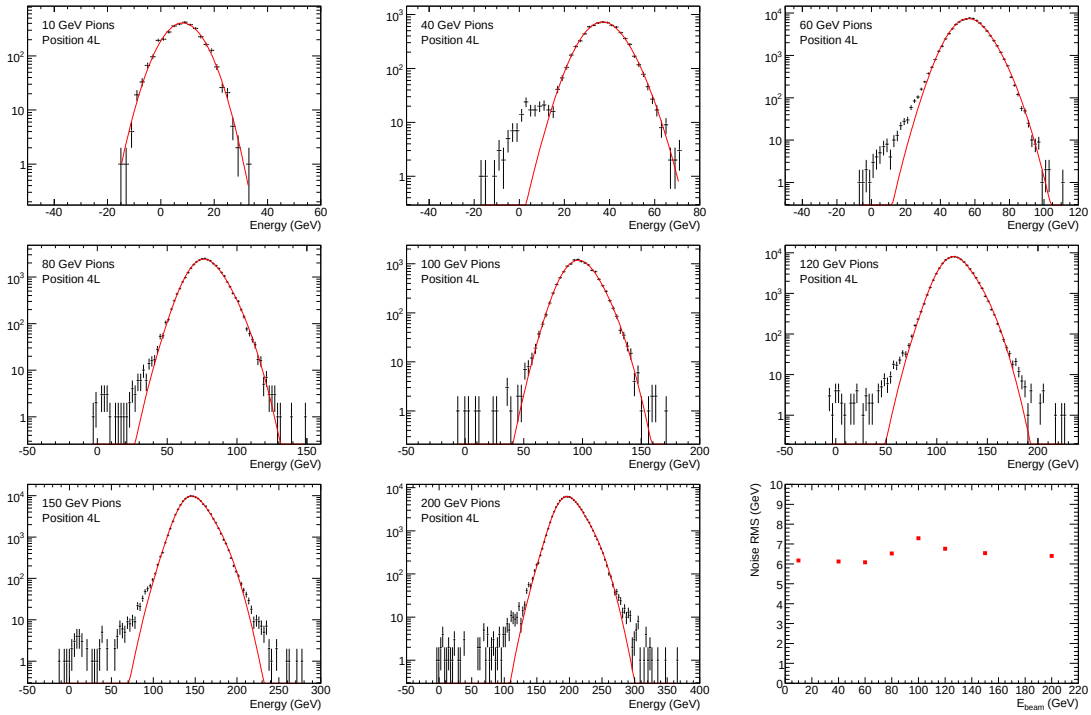

Figure 10. Distributions of reconstructed energy for pions selected from the hadronic data taken at the 4L position, obtained using the flat-weighting technique. Also shown (bottom right) is a plot of the reconstructed noise at each 4L energy point, obtained in the manner described in the text.

weights derived from the 200 GeV data at the relevant impact point. Also shown in the lower right plot of each figure is the average reconstructed noise at each beam energy (obtained from random-trigger events in the corresponding datasets). From these distributions the FCal energy response and resolution function for pions are derived. Several methods have been used; the mean and width of the distributions have been taken directly from the observed distributions as well as from fits using a single- and double-Gaussian parametrizations. For the double-Gaussian description, both the four and six parameter fits were performed, as in the analysis of the electron data described in section 3.2. The four parameter double-Gaussian fit results were used to extract the response and resolution results shown below, while the other methods are used in the evaluation of systematic uncertainties. The plots are again presented using a logarithmic scale to illustrate the extent of the tails.

Figure 12 shows the ratio of the reconstructed energy to the beam energy, as a function of the latter, for the 4L and 4H datasets. The upper plots show the results at the EM scale (summed over the three modules), for data and for the three Monte Carlo samples. The lower plots show the calibrated results obtained from data, using flat weights derived from data and from each of the three simulations, in each case from the 200 GeV samples. All hadronic calibration schemes employed by ATLAS are purely Monte Carlo based; these distributions illustrate the degree to which a simple simulation-based calibration scheme reproduces the true particle energy for pions (in this beam test environment). At 200 GeV, calibration using weights derived from the simulation based on the ATLAS default physics list, QGSP_BERT, reconstructs the correct energy to within 2–3%.

2013 JINST 8 P05006

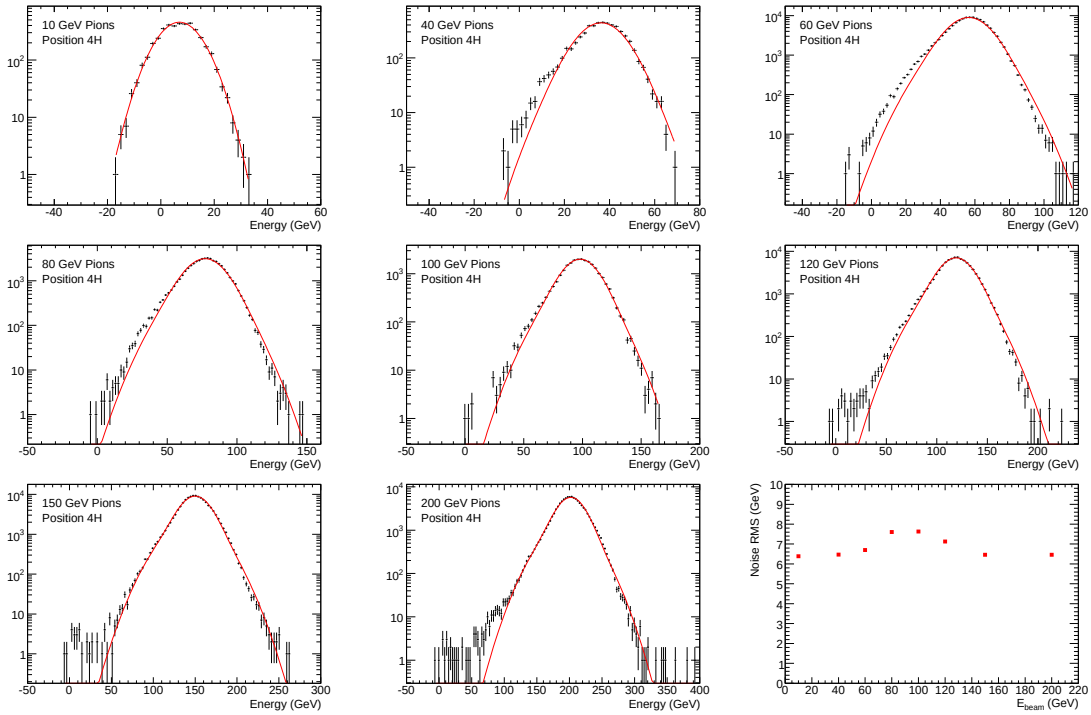

Figure 11. Distributions of reconstructed energy for pions selected from the hadronic data taken at the 4H position, obtained using the flat-weighting technique. Also shown (bottom right) is a plot of the reconstructed noise at each 4H energy point, obtained in the manner described in the text.

Each of the three sets of MC weights reproduces the correct energy to within 3–4%. A slightly different weighting scheme, based on weights derived only from events in which the deposited EM scale energy exceeds 50 GeV (for 200 GeV data or MC) lowers this variation to 2–3%.

Figure 13 shows the noise-subtracted energy resolution at the calibrated scale as a function of the beam energy, for data and Monte Carlo. In this case, the Monte Carlo results are obtained using the same weights as used for the data. Overlaid in each case is the result of a fit to the resolution parametrization described earlier. For the 4L analysis, the stochastic and constant terms are $(88.0 \pm 2.0)\%\sqrt{\mathrm{GeV}}$ and $(6.8 \pm 0.4)\%$ respectively. These supersede the published values of $(94.2 \pm 1.6)\%\sqrt{\mathrm{GeV}}$ and $(7.5 \pm 0.4)\%$. At position 4H, the stochastic term measured in data increases to $(121 \pm 7)\%\sqrt{\mathrm{GeV}}$; the constant term becomes $(7.1 \pm 1.2)\%$. Quoted uncertainties are dominated by systematics, which are taken as the full range of variation seen with use of the four sets of weights and from variation of the selection criteria and fitting procedures. The fit results for both data and Monte Carlo are summarized in table 2. The agreement between data and Monte Carlo is generally good. For both 4L and 4H, predictions for the stochastic term agree with data to within the total uncertainty, except for the FTFP_BERT prediction at position 4L. For the constant term, the simulation slightly underestimates the result obtained at position 4L, though the prediction from QGSP_BERT is consistent within the systematic uncertainty on the result obtained from data, and the predictions using the other two physics lists differ from data by less than two standard deviations. In contrast to the behaviour seen for electrons the constant term increases at 4H. There is somewhat wider variation in the Monte Carlo predictions for the

2013 JINST 8 P05006

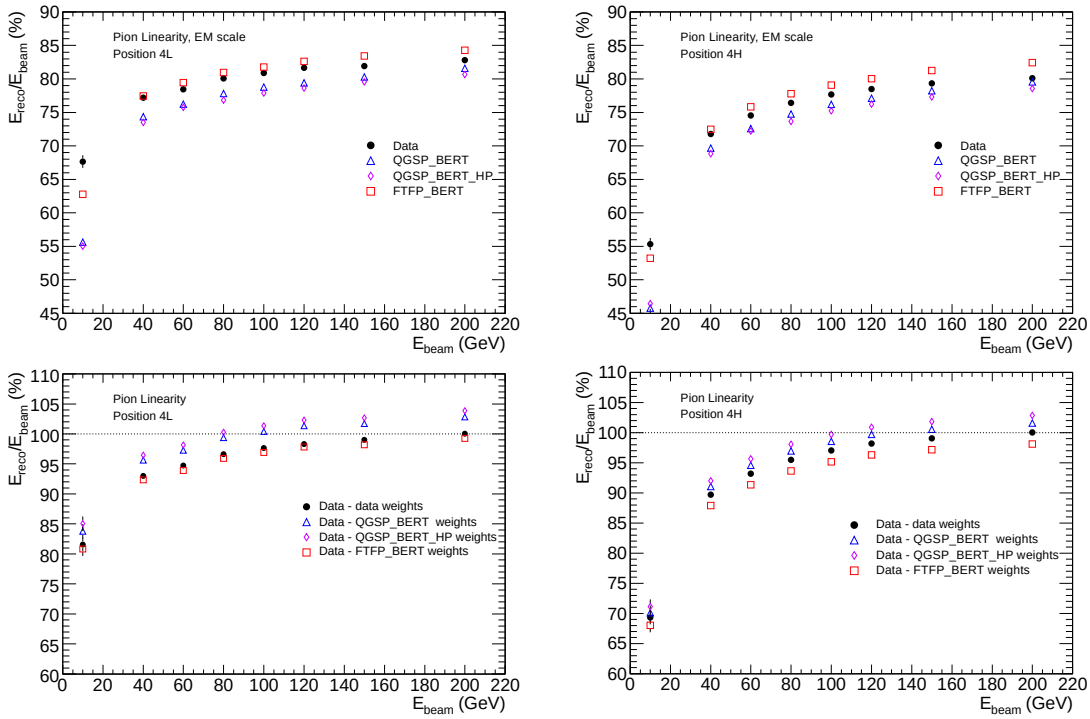

Figure 12. For pions, the relative reconstructed energy, as a function of the beam energy, for data taken at positions 4L and 4H. The upper plots show the results at EM scale, from data and from the three Monte Carlo samples. The lower plots show the results from data only, but calibrated using flat-weights derived from data and from each of the three Monte Carlo samples (in each case using 200 GeV pions).

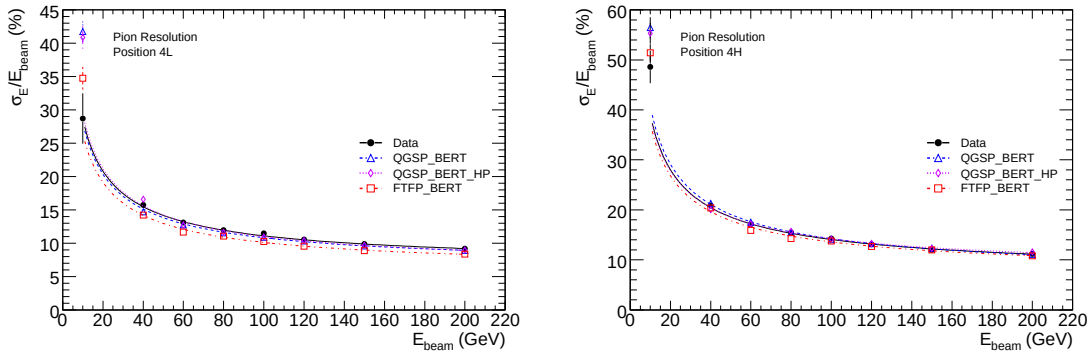

Figure 13. The reconstructed relative (noise-subtracted) energy resolution for pions as a function of the beam energy, at positions 4L and 4H, for data and Monte Carlo. Each dataset is reconstructed using the weights derived from data (200 GeV). The overlaid curves are the results of fits using the parametrization described in the text.

constant term at 4H, but all of the results are consistent with data within the total uncertainty, quoted above. None of the three physics lists provides a clearly superior description of the resolution seen in data.

2013 JINST 8 P05006

Table 2. Pion energy resolution fit results for data and Monte Carlo at 4L and 4H. Quoted uncertainties are statistical only.

	Stochastic term (%$\sqrt{\text{GeV}}$)		Constant term (%)	
	4L	4H	4L	4H
Data	88.0 ± 0.6	120.7 ± 0.6	6.79 ± 0.06	6.98 ± 0.07
QGSP_BERT	86.2 ± 1.1	127.6 ± 1.1	6.54 ± 0.18	6.62 ± 0.17
QGSP_BERT_HP	90.5 ± 1.1	123.3 ± 1.2	6.22 ± 0.13	7.58 ± 0.16
FTFP_BERT	81.2 ± 1.1	119.2 ± 1.1	6.04 ± 0.11	6.77 ± 0.15

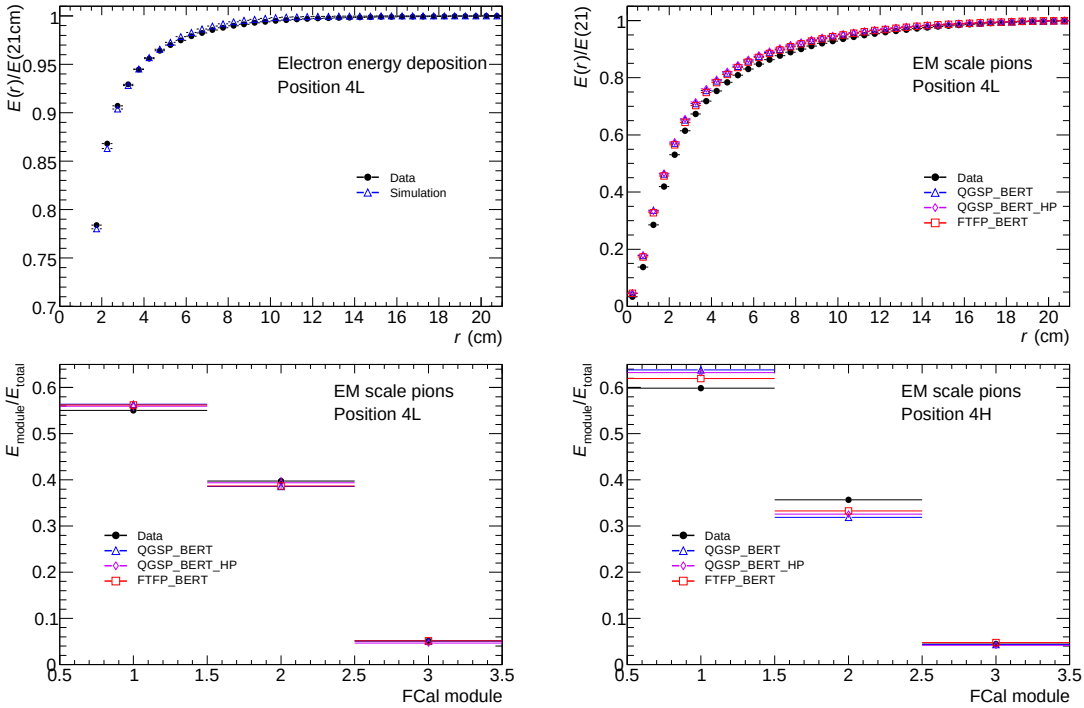

Figure 14. Shower-shape distributions in data and Monte Carlo, for 193.1 GeV electrons and 200 GeV pions. The upper plots are representative of the lateral shower development for electrons and pions and are presented at the EM scale, using data from the 4L position. The lower plots show the sharing of the energy between the three longitudinal layers of the FCal, at both the 4L and 4H positions, again at the electromagnetic scale.

3.4 Validation of simulation of shower shape variables

For validation of the modelling of the showers in the Monte Carlo simulations, the distributions of simple shower shape variables in data and Monte Carlo are shown in figure 14 using the highest-energy electron and pion data. As a measure of the transverse shower profiles, the upper two plots show the (relative) clustered energy for electrons and pions as a function of the radius used for the cylindrical clustering, for data and Monte Carlo. These plots are obtained using data taken at position 4L. To illustrate the longitudinal shower development for pions, the lower two plots

2013 JINST 8 P05006

show energy sharing (at the EM scale) between the three longitudinal compartments of the FCal, obtained using the nominal (16 cm) cylindrical clustering. This is shown for both the 4L and 4H positions, to illustrate the effect of the additional upstream material.

For electrons the data/MC agreement is good. For pions, comparison of the data and Monte Carlo results leads one to the conclusion that the simulation produces hadronic showers which are both longitudinally and transversely more compact that seen in the data. This is consistent with what is seen in similar studies of other ATLAS calorimeter subsystems [6, 15, 16].

3.5 Energy reconstruction using topological clustering

The ATLAS inner tracking system covers the region $|\eta| < 2.5$. There is no tracking in front of the FCal, so clustering algorithms relying on knowledge of the particle impact point are not feasible. There are two default clustering algorithms used in ATLAS, a sliding-window algorithm that is used for electron and photon reconstruction in the central part of the LAr calorimeter, and a topological clustering algorithm [14] which uses information from all calorimeter systems and is applicable over the full acceptance. In the latter technique, clusters are seeded by calorimeter cells satisfying $|E_{\text{cell}}| > 4\sigma_{\text{noise}}$ where σ_{noise} is the average noise for the cell, obtained cell-by-cell from calibration runs and data. Starting from such a seed cell, all neighbouring cells (in 3D) are added to the cluster. Any of these cells which satisfies $|E_{\text{cell}}| > 2\sigma_{\text{noise}}$ in turn has its neighbour cells added, and this procedure iterates until no cell on the cluster perimeter passes this cut. The thresholds are defined in terms of the absolute cell energies in order to avoid biases. The cluster splitting procedure described in reference [14] is switched off for this analysis.

The topological clustering is performed using cell energies at the electromagnetic scale. In ATLAS, a number of hadronic calibration schemes are subsequently employed, the most comprehensive being the "local hadronic calibration" procedure [17] which attempts to first identify individual topological clusters as either electromagnetic or hadronic in nature, based on various cluster moments, such as the energy density, and then applies corrections to those clusters identified as hadronic, also according to a set of cluster moments. Subsequent steps apply corrections for "out of cluster" energy and energy lost in un-instrumented material.

In the discussion below, the beam-test data are re-analyzed using the topological clustering procedure to reconstruct the EM-scale energy deposits in the FCal. Reconstructed energies are obtained as the sum over all reconstructed clusters. The noise thresholds are set relative to the cell noise levels reconstructed using randomly-triggered events from the same runs being analyzed.

The results obtained for electrons at the 4L and 4H positions are summarized in figures 15 and 16 which, respectively, show the response linearity and resolution. In each case, the simulation results are overlaid. Results of the fits to the resolution distributions are shown in table 3. The stochastic terms are all slightly higher than the corresponding results in table 1, obtained using cylindrical clustering. This is expected since the topological clustering algorithm tends to miss some energy on the outer periphery of the shower due to the thresholds applied. In the local hadronic calibration scheme employed by ATLAS, this energy is corrected for at a later stage of the procedure, but this has not been attempted here.

The EM-scale response to pions as a function of beam energy is compared to Monte Carlo predictions in the upper plots of figure 17 for both the 4L and 4H positions. This is the sum of

2013 JINST 8 P05006

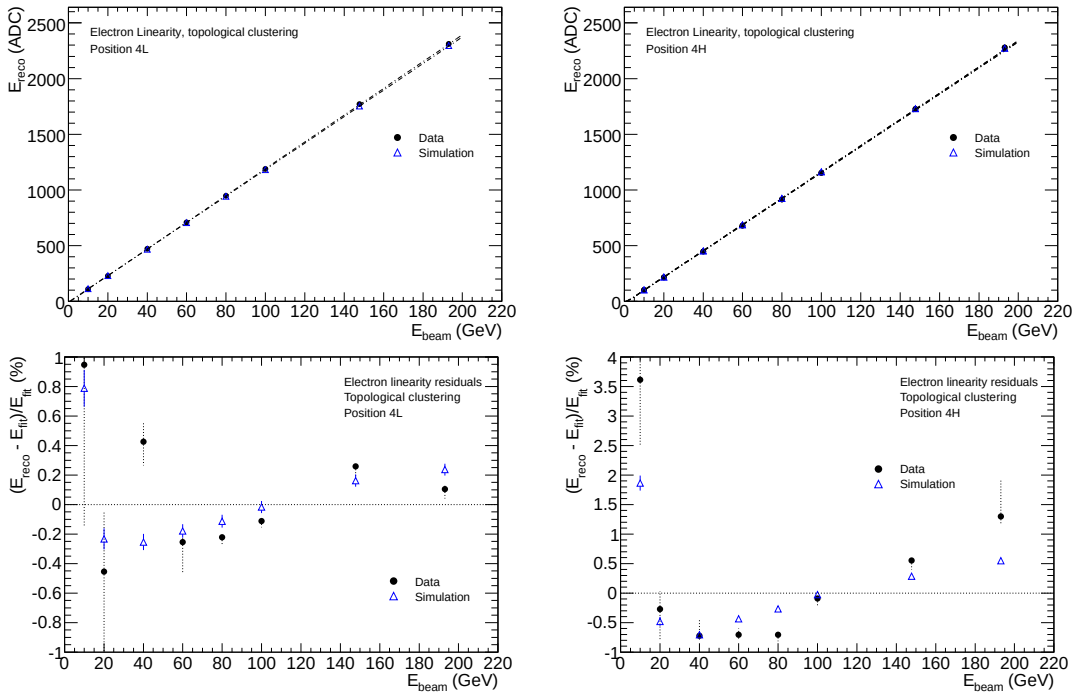

Figure 15. The upper plots show the response linearity for electrons, from analysis of data taken at positions 4L and 4H using topological clustering, with the results of a linear fit overlaid. The lower plots show the corresponding residuals. Monte Carlo predictions are also shown.

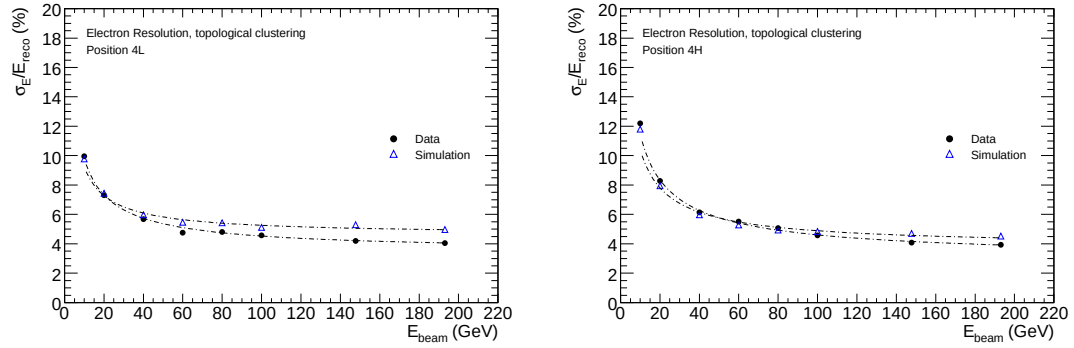

Figure 16. Relative energy resolution for electrons, as a function of beam energy, from analysis of the electron data taken at positions 4L and 4H, using topological clustering. Monte Carlo predictions are also shown, and fit results are overlaid.

the EM-scale energies in the three FCal modules, without weighting. Overall, the best description of both the 4L and 4H data is provided by the QGSP_BERT physics list which, along with QGSP_BERT_HP, slightly underestimates the response. As was the case also with the cylindrical clustering analysis, the FTFP_BERT physics list predicts a higher than observed response for most beam energies, but provides the best description of the lowest energy point, which is significantly underestimated by the two QGSP-based physics lists.

To permit further comparison with the results from section 3.3, these energies are corrected to the hadronic energy scale using the same flat-weighting scheme described earlier, this time

2013 JINST 8 P05006

Table 3. Results of fits to electron energy resolution results for data and Monte Carlo at 4L and 4H, using topological clustering for the energy reconstruction. Quoted errors are statistical only. Systematic uncertainties on the results from data are discussed in the text.

	Stochastic term (%$\sqrt{\text{GeV}}$)		Constant term (%)	
	4L	4H	4L	4H
Data	28.8 ± 0.1	34.8 ± 0.2	3.49 ± 0.02	3.02 ± 0.03
Simulation	25.2 ± 0.3	30.5 ± 0.3	4.62 ± 0.02	3.82 ± 0.03

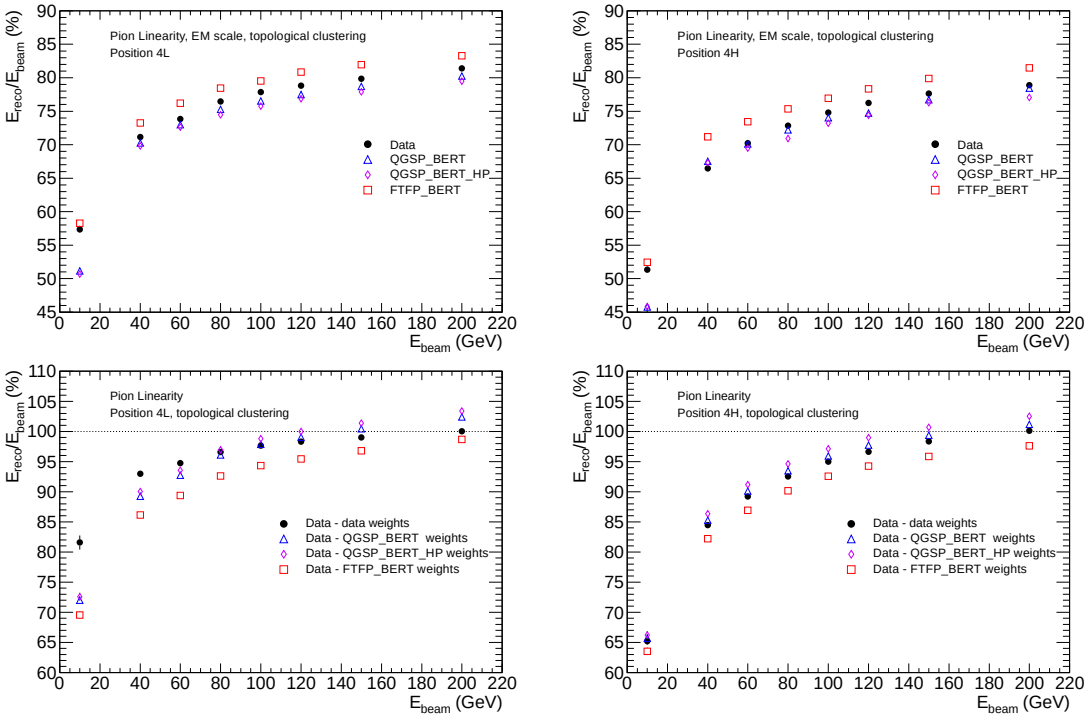

Figure 17. For pions, the relative reconstructed energy, as a function of the beam energy, for data taken at positions 4L and 4H, using topological clustering. The upper plots show the results at EM scale, from data and from the three Monte Carlo samples. The lower plots show the results from data only, but calibrated using flat-weights derived from data and from each of the three Monte Carlo samples (in each case using 200 GeV pions).

with energies reconstructed from topological clusters as input rather than those obtained with the cylindrical clustering method. For this one needs the EM-scale energy in each FCal module. These are obtained by summing over all topological clusters, and assigning the energy of each clustered cell to the module to which it belongs. Based on the EM-scale energies in each module, flat weights are re-derived using the same procedure described earlier; these are again well described by the Monte Carlo, except for the lowest-energy (10 GeV) point. These weights are then used to calibrate the response to the hadronic scale. The results, for data taken at positions 4L and 4H, are shown in the lower plots of figure 17. In each case, the calibration is performed using the weights obtained from data and from each of the three Monte Carlo samples. The Monte Carlo weights

2013 JINST 8 P05006

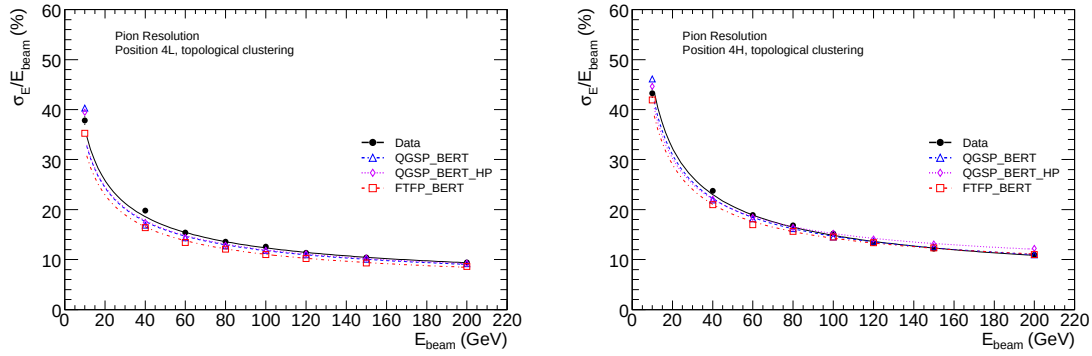

Figure 18. Energy resolution as a function of beam energy for pion data taken at positions 4L and 4H, with energy reconstruction using topological clustering. Monte Carlo predictions are also shown and fit results are overlaid.

Table 4. Pion energy resolution fit results data and Monte Carlo at positions 4L and 4H, based on energy reconstruction using topological clustering and flat-weighting. The quoted uncertainties are statistical only. Systematic uncertainties are described in the text.

	Stochastic term (%$\sqrt{\text{GeV}}$)		Constant term (%)	
	4L	4H	4L	4H
Data	113.5 ± 0.4	143.6 ± 0.4	4.86 ± 0.08	3.80 ± 0.12
QGSP_BERT	107.0 ± 0.7	136.6 ± 0.8	4.97 ± 0.12	5.30 ± 0.17
QGSP_BERT_HP	107.6 ± 0.7	130.1 ± 0.8	5.18 ± 0.12	7.77 ± 0.12
FTFP_BERT	100.7 ± 0.6	126.4 ± 0.7	4.59 ± 0.12	6.62 ± 0.13

reproduce the correct energy within about 3–4%, as was the case with cylindrical clustering. The calibration based on weights obtained using the default ATLAS physics list QGSP_BERT are again within 2–3% of the known beam energy.

The noise-subtracted relative energy resolution as a function of beam energy is shown in figure 18 along with the Monte Carlo predictions (in this case, reconstructed using the same weights as for the data). The results of fits to the usual parametrization are overlaid, and the stochastic and constant terms obtained for data and Monte Carlo are summarized in table 4. Overall, there is a reasonable description of the resolution at both the 4L and 4H positions, though the constant term obtained from the beam-test data is again lower than in the Monte Carlo. This is particularly evident at 4H where the data indicate a lower constant term than at 4L, while all three simulations predict an increase. Both QGSP_BERT and FTFP_BERT provide a good description of the relative increase in the stochastic term due to the additional upstream material at the 4H position.

3.6 Study of energy containment at high $|\eta|$

The beam-test discussed here had one additional goal, which was the study of energy containment near the high $|\eta|$ edge of the FCal. This study was undertaken only with the 200 GeV pions, at positions 1, 2 and 3. The aim was to understand the energy losses of high-energy particles, either due to leakage down, or splashing across, the beam hole. In the analysis described below, the recon-

2013 JINST 8 P05006

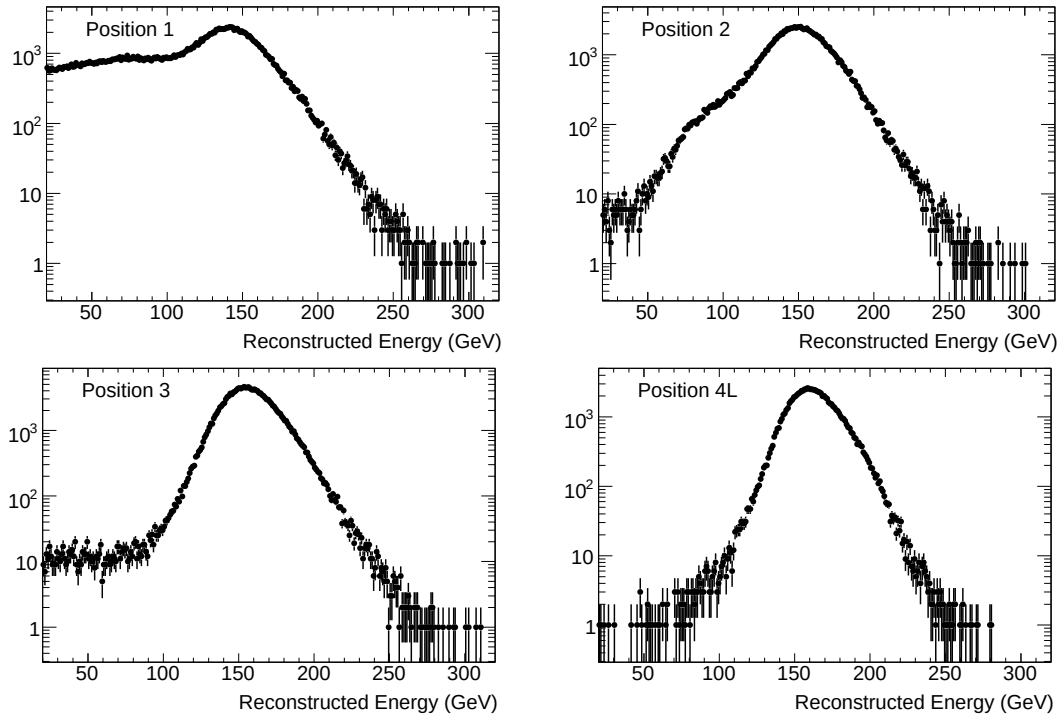

Figure 19. The total clustered energy at the EM scale (FCal1+FCal2+FCal3) for 200 GeV pions at positions 1, 2, 3 and 4L.

structed energy is the sum of the energies from all reconstructed topological clusters. As described earlier, the topological clustering algorithm relies on knowledge of each cell's nearest neighbours. Cells located across the beam hole from one another are not treated as nearest neighbours, so energy that splashes across the beam hole will not be clustered with the main energy deposit unless there is a path of neighbour cells along the inner radius that connects the two regions. Energy deposited in this way could form part of a separate cluster, but that will not necessarily be the case. While the study was originally undertaken in the hope of deriving corrections to cluster energies at high-$|\eta|$, the results presented here are offered only to demonstrate that the performance in this region is reasonably well modelled by the Monte Carlo simulation.

In this high-$|\eta|$ region the response distribution is sensitive to local variations in the beam profile, since particles close to the inner edge deposit only part of their energy in the detector, with the fraction depending on the distance from the inner edge. For this reason, the simulation used for this study varied slightly from the one described earlier in the paper in that the beam profiles used for the event generation were taken from data rather than treated as uniform. The reconstructed energy spectra (at the electromagnetic scale) at the three points are shown in figure 19 along with the corresponding energy spectrum obtained from data at position 4L, for comparison. At position 3 one sees a peak consistent with the one observed at 4L, but with an enhanced population of the low energy tail. At position 2 the response is smeared out even further: note that the shoulder seen in this distribution at about 70–80 GeV is attributable to a non-uniform beamspot population. At position 1 the tail to low energies is higher still. Moving from position 4 to position 1, one also sees, at each stage, a small downward shift in the location of the main peak.

2013 JINST 8 P05006

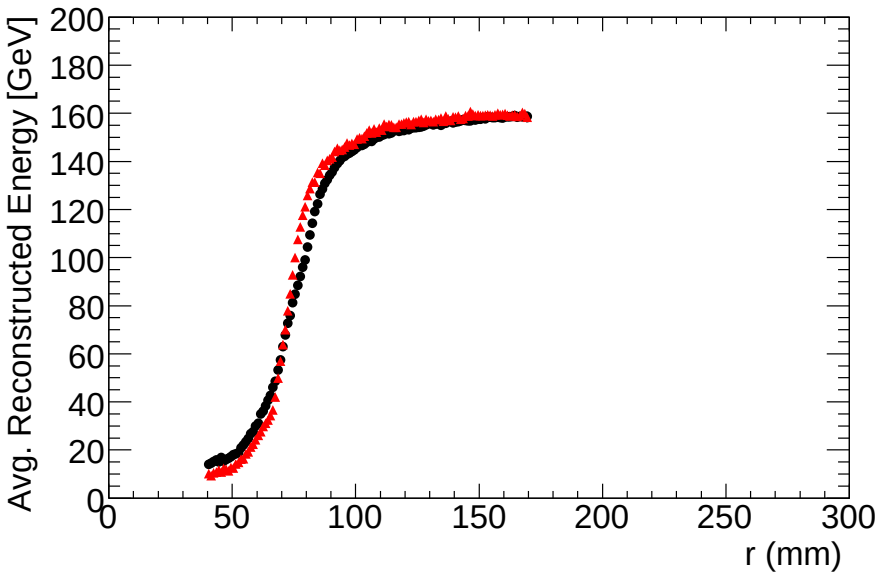

Figure 20. The mean reconstructed energy as a function of the radial distance (from the beamline) of the beam-particle impact point on the face of the FCal1 module, for 200 GeV pions. Beam-test data are shown as dark circles while Monte Carlo is shown as lighter triangles. For the simulation, the true impact point is used. These results are at the EM scale and are obtained from analysis of the data taken at points 1, 2 and 3, and the corresponding simulations using QGSP_BERT, which is the default physics list for ATLAS simulations.

An analysis of the data from points 1, 2 and 3, using the tracking information from the BPCs, allows determination of the mean reconstructed energy for 200 GeV pions as a function of radial distance of the beam-particle impact point from the beamline. This is shown in figure 20 for both data and Monte Carlo: for the latter, the true impact point is used.[2] One sees a reasonable agreement between the data and the Monte Carlo, which was generated using the QGSP_BERT physics list.

4 Comparison to other beam test results

The response of the FCal to electrons and pions has also been investigated using data taken during the 2004 endcap combined beam test, which was primarily intended for investigation of the combined performance of the endcap and forward calorimeter systems. The setup used refurbished beam-test modules of the Electromagnetic Endcap Calorimeter (EMEC), FCal1 and FCal2, and special purpose-built modules for the Hadronic Endcap Calorimeter (HEC). Due to a lack of space in the H6 cryostat there was no FCal3 module.[3] The setup included a detailed mockup of the endcap cryostat material upstream of, and between, the calorimeter modules, including the cryostat bulkhead in front of the FCal1 module, the FCal support tube, and the projective forward cone illustrated in figure 2. The JM shielding was not modelled. The gap between the cryostat bulkhead

[2] The resolution on the beam-impact point reconstructed from the BPC information is $\lesssim 1$ mm, so is not expected to affect this distribution dramatically; however, this effect was not included in the simulation.

[3] There was, instead, a small parallel-plate copper/LAr calorimeter installed behind the FCal2 module. However, this was not used in the analysis of those data.

2013 JINST 8 P05006

and the FCal1 module front face was the nominal value of 29 mm. At one beam-impact point in the FCal (corresponding to $|\eta| \approx 3.6$), electron and pion energy scans were performed over the same range of energies investigated here.

The data from the 2004 beam test have, in particular, been used to investigate the energy sharing in the overlap region between the endcap and forward calorimeters, and to study the performance of the local hadronic calibration (LC) procedure that was described briefly in section 3.5 [7]. Derivation of the local hadronic calibration constants depends on an accurate modelling of both the detector and the upstream materials, since the calibration constants are derived entirely from Monte Carlo. Such a calibration was not attempted for the FCal standalone beam test. However, for comparison to the results obtained from the endcap combined beam test some of the cluster quantities most relevant to the local hadronic calibration procedure have been investigated here, using the production modules that are now operating in ATLAS.

The scheme used by the LC procedure to classify topological clusters as electromagnetic or hadronic relies heavily on the cluster energy density ρ and the cluster depth λ_c [17]. The distributions of these quantities reconstructed from the 193.1 GeV electrons and 200 GeV pion data sets, at point 4H, are shown in figure 21. In each case, data are shown along with the Monte Carlo predictions. The distributions obtained from the electron data show good agreement with Monte Carlo. The pion distributions are less well reproduced, but the distributions here are very similar to those obtained from the combined beam test, for both data and Monte Carlo [7].

The response linearity and resolution results obtained in this paper using topological clustering and flat-weighting are consistent with the results obtained from an analysis of the 2004 beam-test data, which are based on the local hadronic calibration, using topological clustering (and hence do not rely on knowledge of the beam impact point). The setups for the two beam tests differed, making direct comparison of the results difficult. However, the EM-scale pion response results (see figure 17) for the 4H data agree well with similar results obtained in the 2004 beam test (see figure 24 of reference [7]). The hadronic resolution results obtained in reference [7] are similar to those obtained here from analysis of the 4L data, so better than those obtained at 4H. However, for the 2004 beam test, the JM moderator was not modelled. Also, with its refined corrections for effects not considered here, one might expect that the LC-based analysis would yield results superior to those obtained here at the 4H position. Furthermore, the presence of the additional LAr volume in front of the FCal1 front face, in the beam-test setup described here, results in a slightly larger stochastic term than would be the case without it. Simulation results predict that the stochastic term for electrons drops by about 2% (absolute) if the thickess of this volume is reduced to the nominal value of 29 mm. For pions the reduction is about 4–5%. The values of the constant terms are not significantly affected.

5 Summary and conclusions

The FCal detector for one side of ATLAS has been tested with electron and hadron beams in the energy region of about 10–200 GeV. Previously published results demonstrate that the intrinsic FCal performance meets ATLAS requirements. Nevertheless, slightly improved result are presented here, as the previously published results were affected by a rounding error in the cell-energy calculation. The present paper reports a study of beam-test data taken with material placed in the

2013 JINST 8 P05006

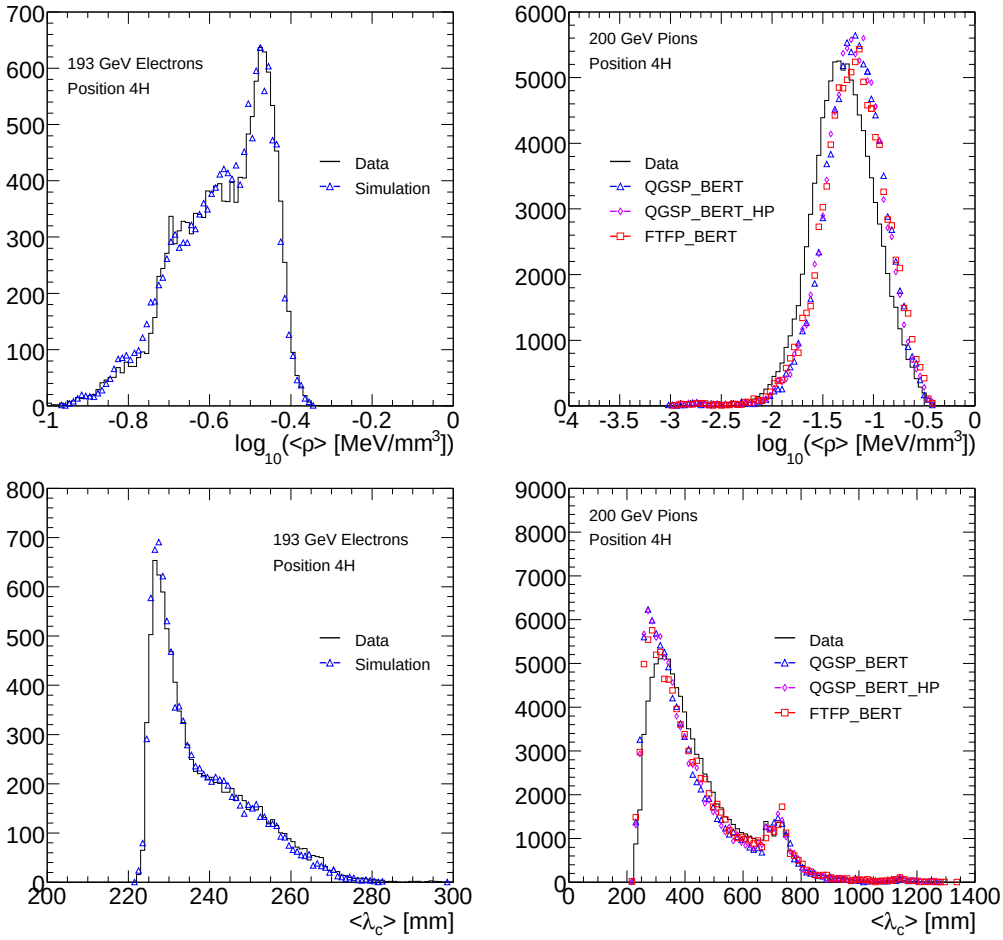

Figure 21. Cluster energy density and cluster depth, for topological clusters reconstructed from pion and electron data at position 4H.

beamline, upstream of the FCal, in order to investigate the effects of such material on the detector performance. The response of the detector to beam particles hitting near the inner edge (high-$|\eta|$ region) of the acceptance is also discussed. For all analyses presented here, the results of detailed Monte Carlo simulations based on GEANT4 are also presented. Simulation results were not available at the time of our previous publication.

The effect of the material upstream of the detector is to slightly degrade the stochastic term of the energy resolution. This is reasonably described by the simulation. The modelled material, however, is only a portion of what is present in ATLAS, so this comparison is relevant mainly as a test of the ability of the Monte Carlo to model such material effects, rather than to quantify the response expected in ATLAS.

All hadronic calibration schemes currently employed by ATLAS are purely Monte Carlo based. The pion data from the beam test described here has been used to show that a simple simulation-based calibration scheme can reproduce the true particle energy for pions (in this beam test environment) to within a few percent. The best results are obtained using the QGSP_BERT physics list, which is the default for ATLAS simulations. At the highest available pion energy

2013 JINST 8 P05006

of 200 GeV, calibration of the data using weights derived from the testbeam simulation based on QGSP_BERT reconstructs the correct energy to within 2–3%. The other physics lists investigated performed almost as well.

The performance of the detector has also been investigated at the high-$|\eta|$ edge. For topological clusters, which are used for object reconstruction in ATLAS, the losses in this region due to leakage out past the FCal acceptance appear to be reasonably well modelled by the simulation. This is important for analyses which utilize the full acceptance of the ATLAS calorimeter: see, for example, reference [18].

Acknowledgments

The support of the CERN staff operating the SPS and the H6 beam line, in particular the frequent assistance of Ilias Efthymiopoulos and Adrian Fabich, is gratefully acknowledged. We thank Jens Spanggaard for his help with the CEDAR. We would also like to thank our colleagues from the ATLAS Liquid Argon Electronics and Cryogenics groups for their invaluable help, with particular thanks to Francesco Lanni and Michael Rijssenbeek. We additionally thank the following people for their contributions: Sing-Leung Cheung, Teresa Embry, Philippe Gravelle, Mohammad Hamidian, Adam Hincks, Liz Inrig, Michael Starr, Kevin Sung, Dan Tompkins, Kenneth Vincent and Manuella Vincter.

This work has been supported by the US Department of Energy (DOE DE-FG02-04ER41298), the Natural Science and Engineering Research Council of Canada, the Russian Federal Agency for Atomic Energy and the Russian Federal Ministry of Education and Science.

References

[1] ATLAS collaboration, *The ATLAS experiment at the CERN Large Hadron Collider*, 2008 *JINST* **3** S08003.

[2] L. Evans and P. Bryant, *LHC Machine*, 2008 *JINST* **3** S08001.

[3] J.P. Archambault et al., *Energy calibration of the ATLAS Liquid Argon Forward Calorimeter*, 2008 *JINST* **3** P02002.

[4] ATLAS collaboration, *Liquid argon calorimeter: technical design report*, CERN/LHCC/96-41 (1996).

[5] A. Artamonov et al., *The ATLAS Forward Calorimeter*, 2008 *JINST* **3** P02010.

[6] J. Pinfold et al., *Performance of the ATLAS liquid argon endcap calorimeter in the pseudorapidity region* $2.5 < |\eta| < 4.0$ *in beam tests*, *Nucl. Instrum. Meth.* **A 593** (2008) 324.

[7] ATLAS LIQUID ARGON ENDCAP collaboration, *Evaluation of the local hadronic calibration with combined beam-test data for the endcap and forward calorimeters of ATLAS in the pseudorapidity region* $2.5 < |\eta| < 4.0$, *Nucl. Instrum. Meth.* **A 693** (2012) 74.

[8] J.C. Armitage et al., *Electron signals in the Forward Calorimeter prototype for ATLAS*, 2007 *JINST* **2** P11001.

[9] C. Bovet, R. Maleyran, L. Piemontese, A. Placci and M. Placidi, *The CEDAR counters for particle identification in the SPS secondary beams: a description and an operation manual*, CERN Yellow Report CERN-82-13 (1982).

2013 JINST 8 P05006

[10] GEANT4 collaboration, S. Agostinelli et al., *GEANT4: a simulation toolkit*, *Nucl. Instrum. Meth.* **A 506** (2003) 250.

[11] J.P. Archambault et al., *The simulation of the ATLAS Liquid Argon Calorimetry*, ATLAS-LARG-PUB-2009-001-1 (2009).

[12] W.E. Cleland and E.G. Stern, *Signal processing considerations for liquid ionization calorimeters in a high rate environment*, *Nucl. Instrum. Meth.* **A 338** (1994) 467.

[13] P. Speckmayer, *Impact of the choice of physics list on GEANT4 simulations of hadronic showers in tungsten*, LCD-Note-2010-002 (2010).

[14] W. Lampl et al., *Calorimeter clustering algorithms: description and performance*, ATL-LARG-PUB-2008-002 (2008).

[15] K.-J. Grahn, A. Kiryunin and G. Pospelov, *Tests of local hadronic calibration approches in ATLAS combined beam tests*, *J. Phys. Conf. Series* **293** (2011) 012032.

[16] ATLAS collaboration, *Response and shower topology of 2 to 180 GeV pions measured with the ATLAS barrel calorimeter at the CERN test-beam and comparison to Monte Carlo simulations*, ATL-CAL-PUB-2010-001 (2010).

[17] T. Barillari et al., *Local hadronic calibration*, ATL-LARG-PUB-2009-001-2 (2009).

[18] ATLAS collaboration, *Measurements of the pseudorapidity dependence of the total transverse energy in proton-proton collisions at* $\sqrt{s} = 7$ *TeV with ATLAS*, *JHEP* **11** (2012) 033.

2013 JINST 8 P05006